© 2022 Hefei Institutes of Physical Science, Chinese Academy of Sciences and IOP Publishing Printed in China and the UK

Plasma Sci. Technol. **24** (2022) 124009 (11pp) https://doi.org/10.1088/2058-6272/aca272

Overview of runaway current suppression and dissipation on J-TEXT tokamak

Zhongyong CHEN (陈忠勇)[1], **Zhifang LIN** (林志芳)[1,2,*], **Wei YAN** (严伟)[1,*], **Duwei HUANG** (黄都伟)[1], **Yunong WEI** (魏禹农)[1], **You LI** (李由)[1], **Nianheng CAI** (蔡念恒)[1], **Jie HU** (胡捷)[1], **Yonghua DING** (丁永华)[1], **Yunfeng LIANG** (梁云峰)[1], **Zhonghe JIANG** (江中和)[1] **and J-TEXT Team**[1,3]

[1] International Joint Research Laboratory of Magnetic Confinement Fusion and Plasma Physics, State Key Laboratory of Advanced Electromagnetic Engineering and Technology, School of Electrical and Electronic Engineering, Huazhong University of Science and Technology, Wuhan 430074, People's Republic of China
[2] School of Electrical Engineering & Automation, Jiangsu Normal University, Xuzhou 221116, People's Republic of China

E-mail: zflin@jsnu.edu.cn and yanwei1090@hust.edu.cn

Received 29 August 2022, revised 10 November 2022
Accepted for publication 14 November 2022
Published 22 December 2022

Abstract

The main works on disruption mitigation including suppression and mitigation of runaway current on the J-TEXT tokamak are summarized in this paper. Two strategies for the mitigation of runaway electron (RE) beams are applied in experiments. The first strategy enables the REs to be completely suppressed by means of supersonic molecular beam injection and resonant magnetic perturbation which can enhance RE loss, magnetic energy transfer which can reduce the electric field, and secondary massive gas injection (MGI) which can increase the collisional damping. For the second strategy, the runaway current is allowed to form but should be dissipated or soft landed within tolerance. It is observed that the runaway current can be significantly dissipated by MGI, and the dissipation rate increases with the injected impurity particle number and eventually stabilizes at 28 MA s^{-1}. The dissipation rate of the runaway current can be up to 3 MA s^{-1} by ohmic field. Shattered pellet injection has been chosen as the main disruption mitigation method, which has the capability of injecting material deeper into the plasma for higher density assimilation when compared to MGI. Moreover, simulation works show that the RE seeds in the plasma are strongly influenced under different phases and sizes of $2/1$ mode locked islands during thermal quench. The robust runaway suppression and runaway current dissipation provide an important insight on the disruption mitigation for future large tokamaks.

Keywords: tokamak, disruption mitigation, runaway electron, runaway current

(Some figures may appear in colour only in the online journal)

1. Introduction

A disruption is a sudden termination of plasma discharge, which not only results in large thermal loading and electromagnetic force on the surrounding structures, but also generates runaway electrons (REs) which can burn holes through structures [1–3]. Thus, the avoidance and mitigation of disruption is a critical issue for the safe operation of tokamaks. Both the thermal loads and electromagnetic force have been mitigated with a certain amount of impurities by massive material injection systems, like massive gas injection (MGI) [4, 5] and shattered pellet injection (SPI) [6]. For ITER, MGI may have a better mitigation effect on heat load and halo current. However, the suppression of REs remains

* Authors to whom any correspondence should be addressed.
[3] See Nengchao Wang *et al* 2022 (https://doi.org/10.1088/1741-4326/ac3aff) for the J-TEXT tokamak.

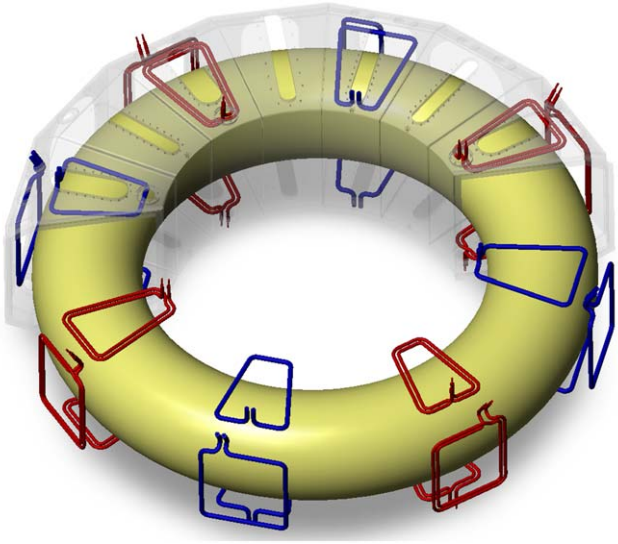

Figure 1. Layout of the RMP coils on J-TEXT. Reproduced courtesy of IAEA. Figure from [12]. Copyright (2019) IAEA.

uncertain because a large runaway current will be formed even if only a few RE seeds survive during disruption. According to the calculation for ITER, plasma disruption generates a runaway current of up to 10 MA, with an energy of tens of MeV [7, 8]. Thus, the mitigation and suppression of runaway currents have become high priority tasks to address for future tokamaks. Both experimental and modeling efforts focus on the understanding of the physics behind and the technology exploration.

The J-TEXT tokamak is a conventional tokamak with an iron core [9], which has been equipped with disruption mitigation systems including MGI, SPI, resonant magnetic penetration (RMP) and magnetic energy transfer (MET). J-TEXT tokamak is convenient for the disruption mitigation studies. In the last few years, the most significant results of disruption mitigation on J-TEXT have included suppression of REs by mitigation systems (SMBI, RMP, MGI and MET), dissipation of runaway current by MGI, OH field and SPI, and simulations of the suppression of REs during disruption. Thus, the rest of this paper is organized as follows. Section 2 describes the disruption mitigation systems and the diagnostics using in the experiment. Sections 3 and 4 summarize the recent progress on disruption mitigating experiments, and the simulation results are presented in section 5. Finally, section 6 gives a summary and outlook.

2. Disruption mitigation systems

It is difficult to generate runaway current naturally on the J-TEXT tokamak, and the MGI of Ar is beneficial for the formation of runaway current. Thus, two MGI valves have been developed on J-TEXT [10]. One of the MGI valves with 30 ml at the bottom of port 9 has been used to trigger major disruption and obtain a stable runaway current. Another MGI valve with 60 ml at the top of port 9 has been applied to dissipate the runaway current. As shown in figure 1, the RMP coils [11, 12] are installed inside the vessel to generate magnetic perturbations with different pure mode structures, which is beneficial for disruption mitigation research. The SPI system [13] is installed in the horizontal window of port 10, which can inject Ar pellets with diameter of 5 mm and length of less than 10 mm. Its structure is shown in figure 2. The supersonic molecular beam injection (SMBI) system has also been used to generate magnetic perturbations by injecting different supersonic gases [14]. The number of injected particles can be adjusted by varying the gas pressure and pulse width. The MET system uses a set of coils as energy transfer coils (ETCs), which are installed outside the vacuum vessel (VV) and distributed symmetrically to the mid-plane [15, 16]. A schematic of the MET is presented in figure 3. A thyristor has been selected as the controlling switch (CS). EAU in the figure represents the energy absorbing unit. The ETCs are strongly magnetically coupled with plasma; when the controlling switch is triggered during the disruptions, plasma current rapid shutdown induces a co-current in the ETCs, and consumes the plasma poloidal magnetic energy by the EAU.

In addition, the diagnostics applied for detecting the basic parameters of plasma and REs have been equipped on J-TEXT. The electron density is measured by a multi-channel polarimeter interferometer (POLARIS), which views the plasma vertically with 17 channels ranging from $r = -24$ to $+24$ cm [17]. The poloidal and toroidal Mirnov arrays are used to obtain the magnetohydrodynamic (MHD) activities [18], and the plasma temperature is measured by the electron cyclotron emission (ECE) system which has a spatial resolution of 1 cm after upgrade [19, 20]. The hard x-ray radiation (HXR) from REs can be detected by NaI (T1) scintillators which are installed on the equatorial plane to measure the HXR in the energy range of 0.5–10 MeV [21], and four extreme ultraviolet (AXUV) arrays are arranged on ports 3, 5, 6, and 13, which can be used to measure the radiation power [22]. The locations of all the diagnostics and disruption mitigation systems on J-TEXT are shown in figure 4.

3. Suppression of REs

During disruption, thermal quench (TQ) leads to a rapid decrease in plasma temperature, resulting in an increase in plasma resistivity. Consequently, a large electric field parallel to the magnetic field $E_{||}$ is induced which prevents the plasma current from decaying rapidly and strives to maintain the pre-disruption plasma current. This $E_{||}$ continuously accelerates the electrons to run away when the electric field force exceeds the collisional friction force. The critical electric field [23, 24] can be given by $E_c = \frac{e^3 n_e \ln\Lambda}{4\pi\varepsilon_0{}^2 m_e c^2}$, where n_e is the electron density, m_e is the electron mass, e is the electron charge, c is the speed of light, and $\ln\Lambda$ is the Coulomb logarithm. There will be no REs if the electric field less than the E_c, and all electrons will run away if the electric field is larger than the Dreicer field E_D ($>E_c$) [25], where $E_D = \frac{e^3 n_e \ln\Lambda}{4\pi\varepsilon_0{}^2 T_e}$. This mechanism is called the Dreicer generation mechanism, and is one of the primary mechanism of RE generation including

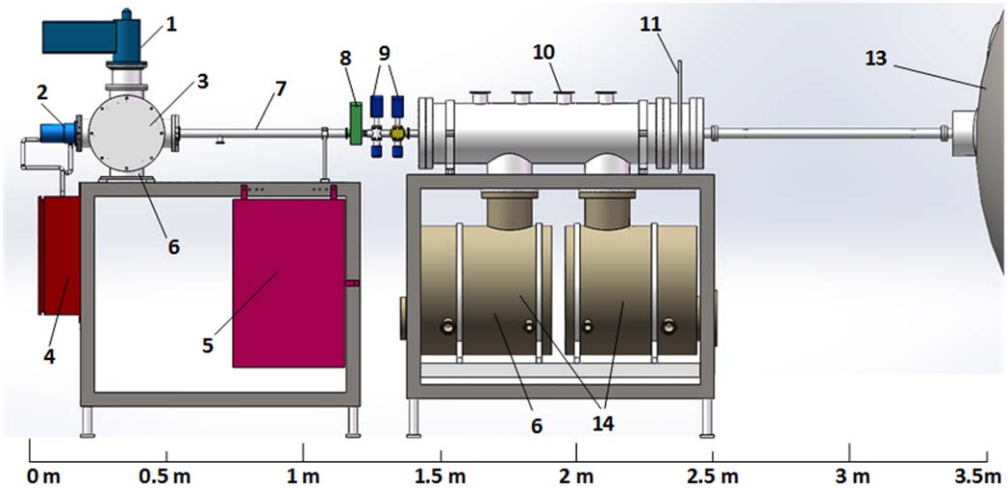

Figure 2. Schematic of the structure of the SPI on J-TEXT; each component can be referred to [13]. Reprinted from [13], with the permission of AIP Publishing.

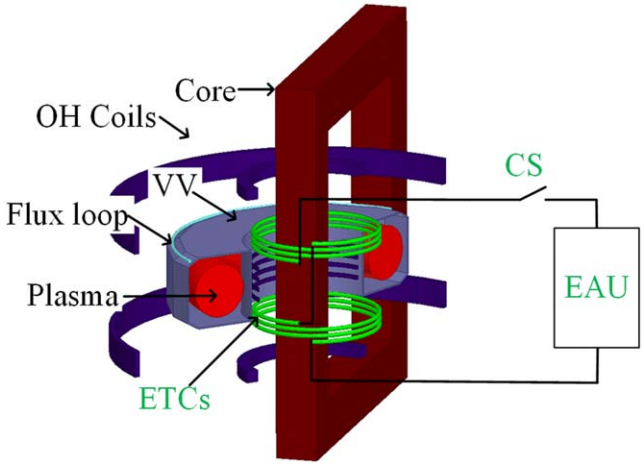

Figure 3. Schematic of MET in J-TEXT. Reprinted from [16], Copyright (2021), with permission from Elsevier.

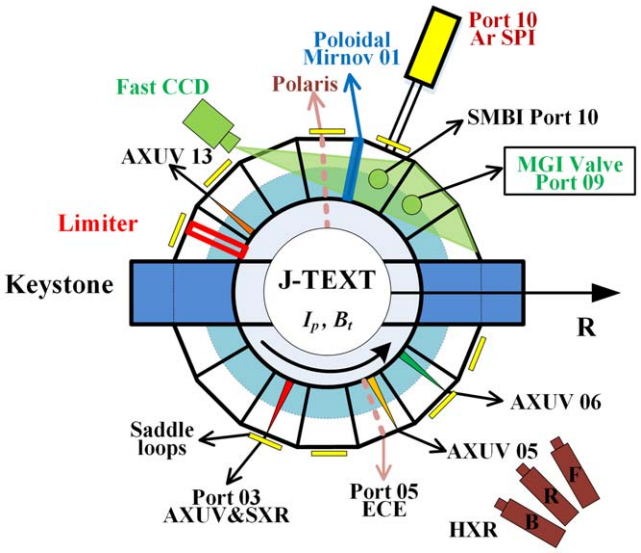

Figure 4. Top view of the locations of diagnostics and disruption mitigation systems on J-TEXT.

tritium decay, Compton scattering and the hot tail process [7]. The tritium decay and Compton scattering have not been experimentally observed yet but they are thought to contribute to the generation of RE seeds in the ITER D–T operation phase. The Dreicer generation mechanism is competitive in many present tokamaks, but is insignificant in the ITER post-disruption condition [7]. The hot tail process is foreseen to be the main primary generation mechanism in ITER if the duration of the TQ is around 1 ms [26]. All the processes of primary mechanism contribute to the generation of RE seeds during the TQ phase. After that, a further growth of RE population is found via knock-on collisions between bulk and existing REs, which gives rise to the runaway current eventually dominating the ohmic current [27]. This generation mechanism of REs is called the second generation mechanism or avalanche mechanism, and it is thought to be one of the dominant mechanisms in the generation of REs in ITER. The generation rate of REs based on the avalanche mechanism is related to the ratio E/E_c; when $E/E_c < 1$ there is no avalanche multiplication [27]. Thus, E_c is the critical electrical field which determines whether the avalanche grows or not. Because E_c is proportional to the electron density n_e, increasing n_e to a critical level can be a feasible method to suppress the generation of REs during disruption. This critical n_e is called the Rosenbluth density which has been estimated to be 4.2×10^{22} m^{-3} for $E_c = 38\,V\,m^{-1}$ in ITER [2]. However, only about 20% of the Rosenbluth critical density has been achieved in experiments to date [28], and the efficiency of gas injection is so weak that most of the impurities have not assimilated with the plasma at the end of the current quench (CQ). Thus, there are still many technical improvements and physical explorations for the suppression of REs that should be solved in the future.

Two strategies for the avoidance and mitigation of REs have been presented in J-TEXT. The safest way is to suppress REs completely. Based on progress in the generation of REs, the REs can be prevented by (a) injecting massive amounts of impurities (gas or pellets), increasing the collisional damping to overcome the accelerated force, (b) applying magnetic

perturbations to destroy the magnetic surfaces, enhancing the RE losses before they are amplified, and (c) declining the parallel electric field $E_{||}$ by a passive mitigation method of magnetic energy transfer, which induces a co-current during disruption and leads to the plasma poloidal magnetic energy being transferred outside the VV.

However, runaway currents form if the first strategy for RE suppression fails. Thus, the second strategy must dissipate or soft land the runaway current to minimize damage to the components of the device. The most common methods of dissipation are MGI or SPI. High-Z impurities are chosen to dissipate the runaway current, because they can lead to effective synchrotron radiation, bremsstrahlung radiation losses and a higher induced critical field [24]. Dissipation of runaway current is also achieved via externally applied negative loop voltages, which has a remarkable effect on the decay of runaway current. While promising results have been obtained in small tokamaks, those in other medium- or large-sized devices have not yet been testified. Recently, wave–particle interaction (WPI) has been considered as a potential method to dissipate RE beams [29–31]. It has reduced or suppressed RE avalanches via large pitch angle scattering. However, active WPI remains a challenge because of the wave accessibility and collisional damping during disruption.

Many questions remain to be explored regarding the understanding and application of technology in the mitigation of runaway current, such as the penetration process of impurity, the particle/electron assimilation mechanisms, the MHD fluctuations evolution, the delivery means for deep penetration, the diagnostics which are suitable for the measurement of formation and loss of RE beams, and other auxiliary methods for the mitigation of runaway current. To date, a reliable and effective method extrapolated to ITER is still uncertain because of the diverse results in different devices and the unclear physical mechanisms behind them. More simulation and experimental studies are needed in disruption mitigation and safe operation for ITER and future large fusion devices.

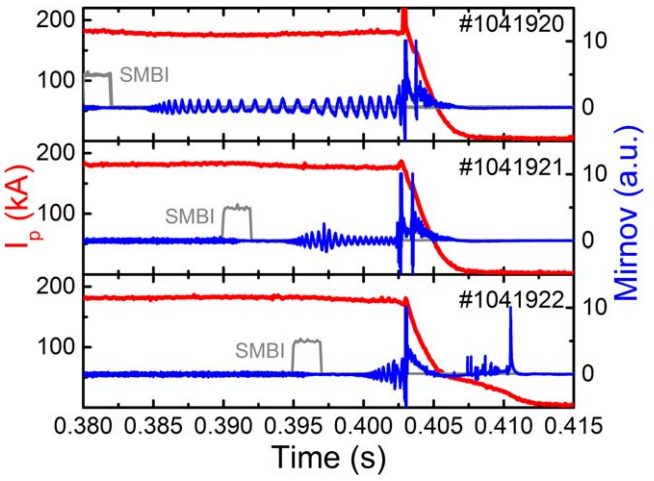

Figure 5. Suppression of runaway current with different SMBI injection times. Reproduced from [34]. © IOP Publishing Ltd. All rights reserved.

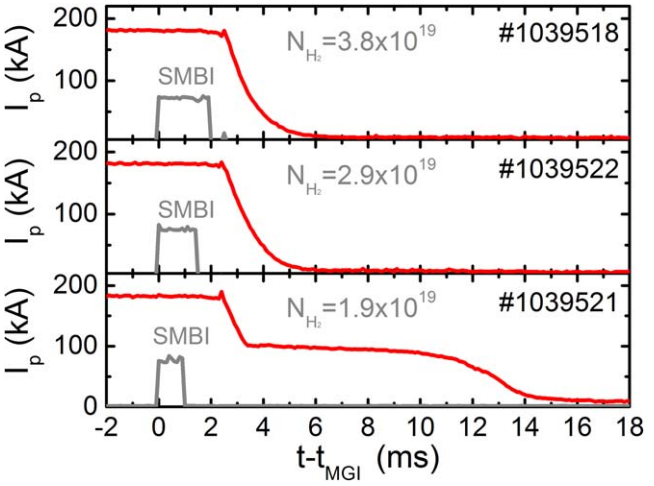

Figure 6. Suppression of runaway current with different SMBI gas quantities. Reproduced from [34]. © IOP Publishing Ltd. All rights reserved.

3.1. Suppression of REs by magnetic perturbations

Magnetic perturbations can change the magnetic topology and deteriorate the RE confinement before the avalanche amplification process. If the loss time of REs is less than the lifetime of REs, the generation of REs will be suppressed, and the loss of REs mainly depends on the stochastization of the magnetic field lines. Thus, promoting stochasticity in the whole plasma cross section by magnetic perturbation is beneficial to the suppression of REs. The TEXTOR and DIII-D tokamaks have demonstrated the availability of this method [32, 33]. In the J-TEXT tokamak, magnetic perturbation is generated by SMBI and RMP.

In the previous experiment, the H_2 SMBI provoked significant magnetic perturbation in the plasma current flattop, and was applied to suppress the generation of REs during disruption phase [34]. It has been demonstrated that the effect on the suppression of REs mostly depended on the H_2 quantity injected and the trigger time of SMBI. Typical results are shown in figures 5 and 6. When the trigger time of SMBI is earlier than the MGI switch time for 5 ms or less, the runaway current is completely avoided. Besides, the suppression of REs has be realized when the number of injected H_2 particles reaches a certain threshold. This phenomenon may be interpreted as the variation of the amplitude and spread region of magnetic perturbation in the plasma. For the case of early SMBI and a large H_2 quantity injection, the magnetic perturbations induced can penetrate further into the plasma center and change the magnetic topology during disruption. The broken magnetic surface in the plasma center leads to a complete suppression of REs. This result may provide a new strategy for the suppression of runaway current in future large tokamaks.

The simplest and effective method of producing magnetic perturbation is external RMP. Thus, the RMP system on J-TEXT is applied to explore the effect of magnetic perturbation on the suppression of REs [35, 36]. It is observed that the runaway current can be fully avoided by applying

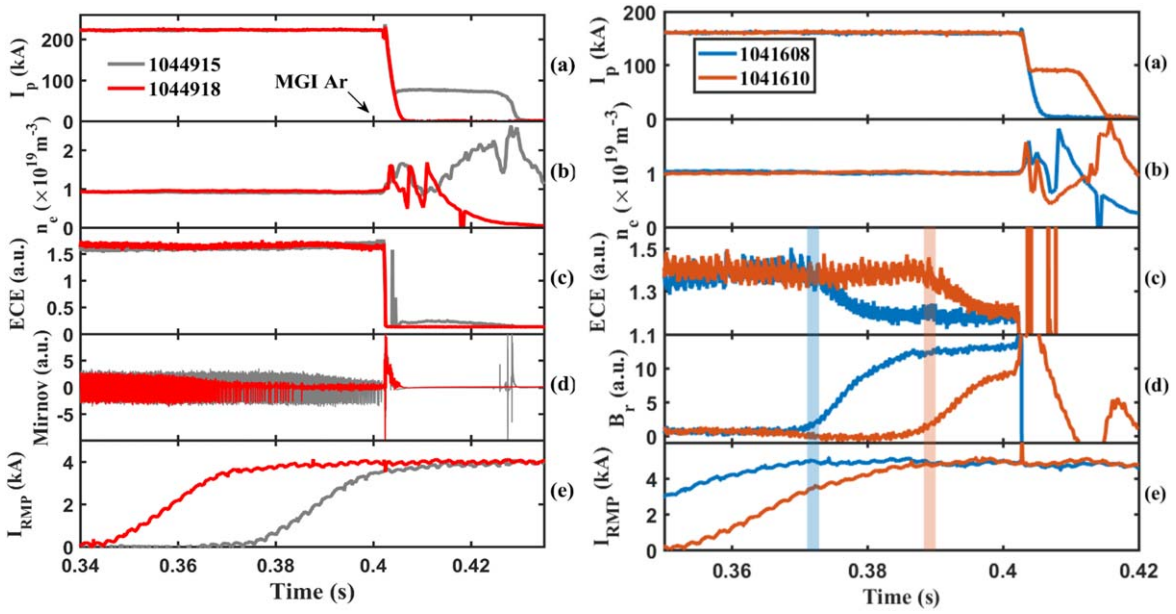

Figure 7. Full suppression of runaway current by mode locking (left) and mode penetration (right). Reproduced courtesy of IAEA. Figure from [35]. Copyright (2018) IAEA. Reproduced from [36]. © IOP Publishing Ltd. All rights reserved.

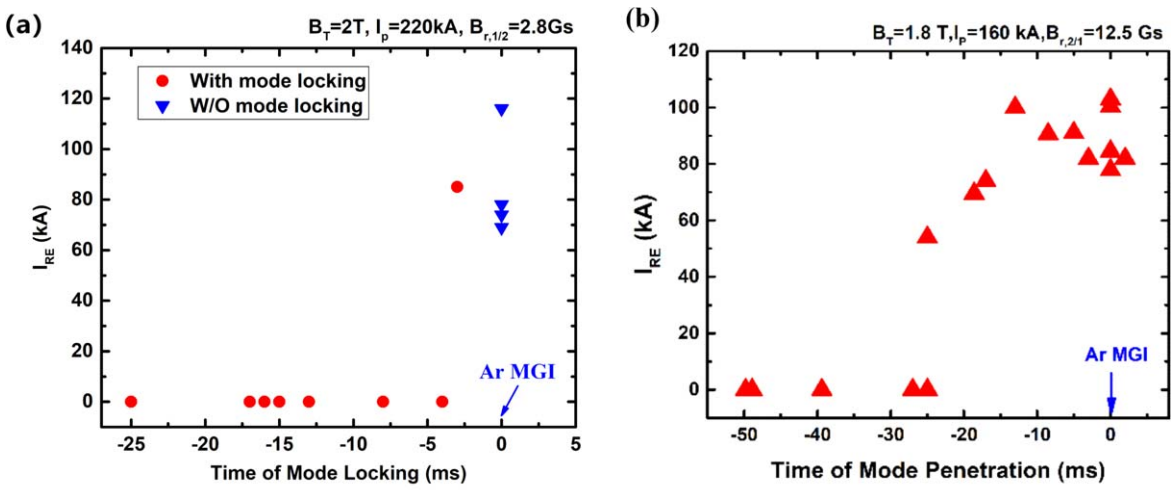

Figure 8. Relationship of the runaway current on the time of (a) mode locking and (b) mode penetration before the disruptions. Reproduced courtesy of IAEA. Figure from [35]. Copyright (2018) IAEA. Reproduced from [36]. © IOP Publishing Ltd. All rights reserved.

$m/n = 2/1$ mode RMP before TQ, as shown in figure 7, and the efficiency of RE suppression is related to the trigger time of RMP (figure 8) which enlarges magnetic islands to form a stronger stochasticity in the whole plasma cross section during disruption. Based on the different plasma conditions with/without MHD activity, two cases are investigated in the J-TEXT tokamak. For the mode locking case, robust suppression of runaway current is reached as long as the mode locking occurs 4 ms before disruption [35], and the runaway current is only partially suppressed with partial mode locking. Stationary magnetic islands result from mode locking, and increase in width over the locking duration until saturation. Thus, a long locking duration, corresponding to a large magnetic island, is more effective at reducing the generation of RE seeds. The NIMROD simulation result shows that the large islands can make a large stochasticity area in the radial distribution of plasma that enhance the RE seed loss and suppress runaway current. For the case without MHD activity in the plasma, the RMP is used to implant magnetic islands before disruption. As the penetration duration increases, the magnetic islands are enlarged to a scale that can suppress generation of REs completely. The island width should be larger than $0.16a$ (a is the minor radius) to realize the suppression of runaway suppression [36]. These results show that the $2/1$ mode islands play an important role in the stochastization of the magnetic field lines during disruption, which is a key point in achieving the suppression of REs and requires further study.

In our experiments, both SMBI and external MPs induced the magnetic perturbation have obvious effect on the suppression of REs. SMBI has the advantage of rapid excitation of magnetic perturbation, but it is difficult to penetrate

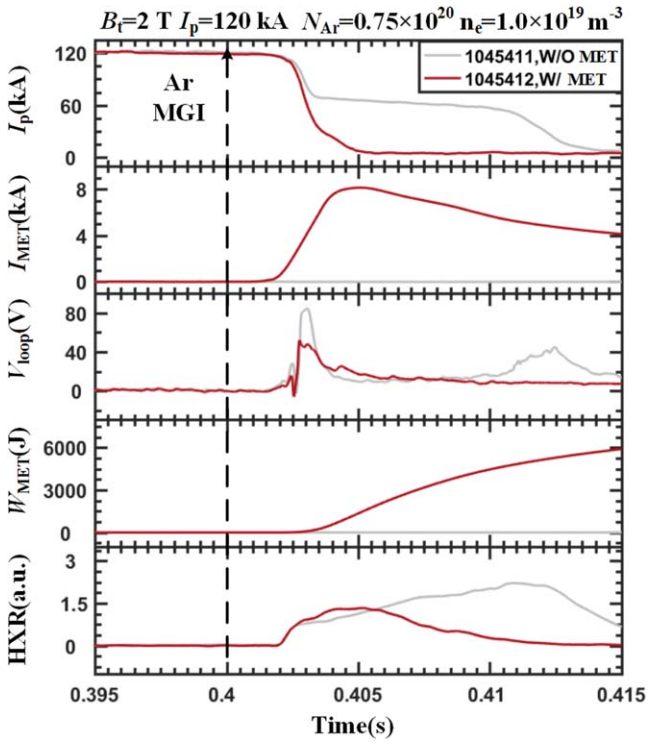

Figure 9. Suppression of runaway current by MET. Reprinted from [16], Copyright (2021), with permission from Elsevier.

into the plasma core under high performance operation. However, RMP can induce magnetic perturbation in the plasma core. Since the RMP coil current needs time to reach sufficient strength, it may not respond to the requirement of disruption mitigation in time.

3.2. Suppression of REs by magnetic energy transfer

Reducing the toroidal electric field by magnetic energy transfer has been studied in J-TEXT. It couples the plasma poloidal magnetic energy during disruption and consumes magnetic energy out of the VV, consequently reducing the runaway kinetic energy significantly so as to suppress runaway current formation during disruption. Almost 20% poloidal magnetic energy can be transferred out and the loop voltage can be reduced maximally 58% [15]. Moreover, the MET system can accelerate the CQ rate and reduce the loop voltage at the same time, as presented in figure 9. As the ETC current increases, the conversion fraction of runaway current significantly decreases, and the runaway current is completely suppressed when I_{ETC} reaches 6.5 kA (figure 10) [16]. The MET provides a new possibility for the magnetic energy transfer and suppression of runaway current during the disruption phase in future devices.

3.3. Suppression of REs by secondary MGI

For the reliable and effective suppression of runaway current, a secondary MGI (MGI2) from another valve with a delay time is performed on J-TEXT [37]. This MGI2 aims to prevent insufficient impurity injection from a single valve and

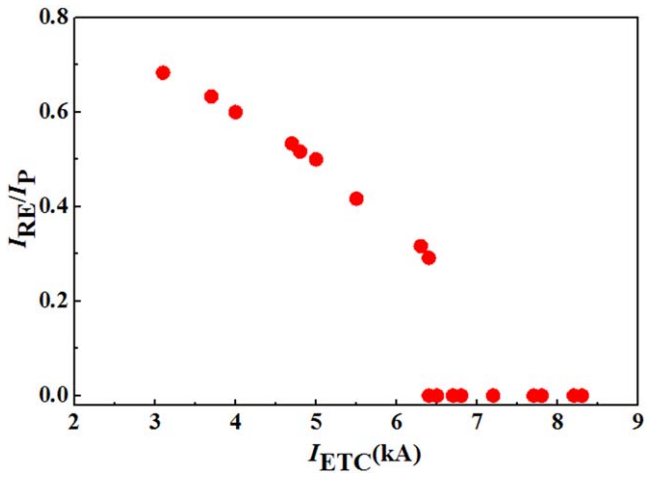

Figure 10. Relationship between ETC current and the ratio of runaway current and plasma current. Reprinted from [16], Copyright (2021), with permission from Elsevier.

increases the electron density to a level that suppresses the generation of REs. The experimental result is shown in figure 11. Runaway current is produced by Ar MGI which is triggered at 0.4 ms, and the impurities used in MGI2 are Ar and Kr (Ar/Kr). It is found that when the secondary impurity gas arrives at the plasma edge before TQ, the generation of runaway current is completely suppressed. However, if the secondary impurity gas arrives at the plasma edge during the CQ phase, the generation of runaway current is partly suppressed. This result may account for the different generation mechanisms of REs during the TQ and CQ phase. During the TQ phase, the primary generation mechanism of REs produces a few RE seeds which are easily suppressed by the increased electron density, consequently resulting in the avoidance of runaway current formation. However, due to the residual RE seeds before the CQ phase, the avalanche mechanism still promotes the formation of runaway current even though the same amount of impurity has been injected. This premier result gives an insight into the runaway current suppression applied in other devices, and it should be noted that the arrival time of sufficient impurity is a key issue in ensuring the efficiency of RE suppression.

4. Dissipation of runaway current

4.1. Dissipation of runaway current by MGI

For a large-scale device, it is difficult to completely suppress the formation of runaway current, and a portion of REs become runaway currents with huge magnetic and kinetic energies during disruption. Thus, dissipating the runaway current is the last resort to ensure the safety of the device. Dissipation of runaway current by high-Z impurities injection is carried out in J-TEXT [38]. A runaway current plateau is induced and formed by the first Ar MGI, and is dissipated by the secondary Ar/Kr MGI. The dissipation efficiency of runaway current, characterized by the decay rate of runaway current (dI_{RE}/dt), is found to increase with the increase in

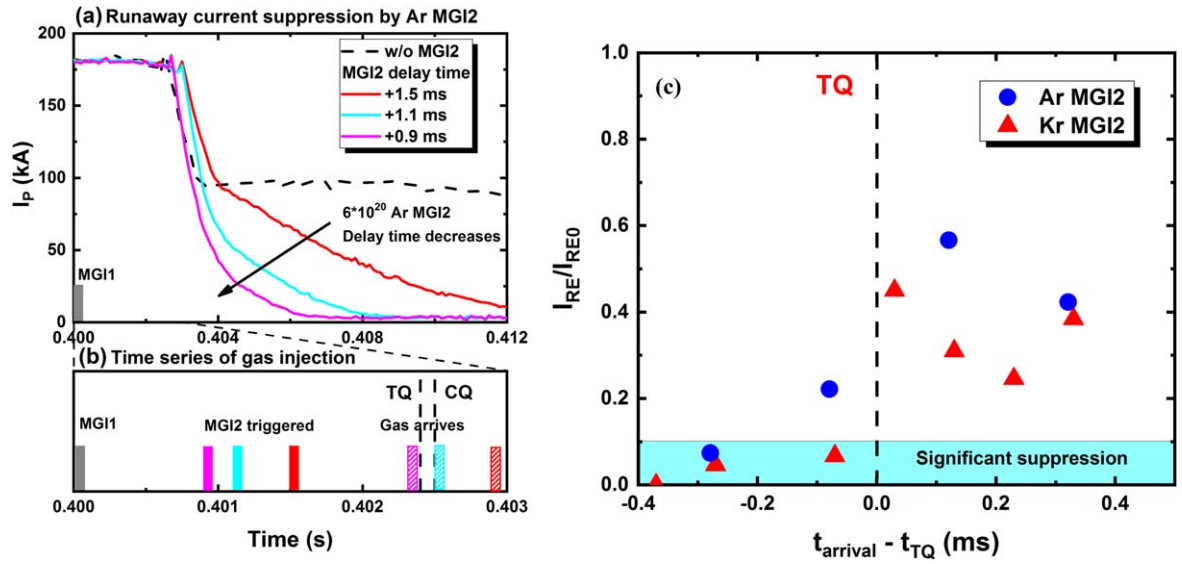

Figure 11. Suppression of runaway current by MGI2 injected with different delay times. (a) Time evolution of current caused by Ar MGI2, (b) time sequence of MGI1 trigger, MGI2 trigger, and MGI2 arriving at the plasma edge, and (c) relationship between runaway currents and the differences between MGI2 arrival times and TQ times of the Ar/Kr cases. Reproduced from [37]. © IOP Publishing Ltd. All rights reserved.

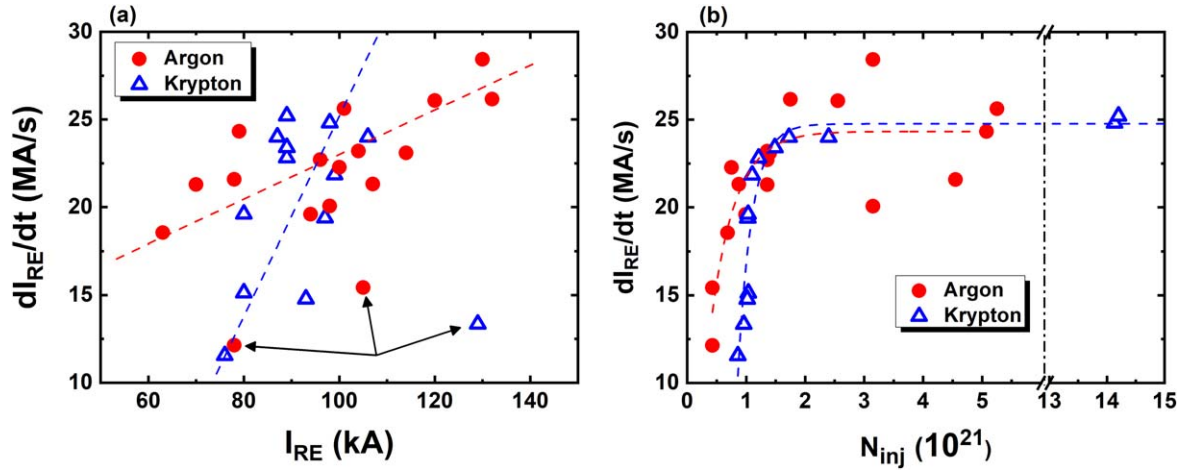

Figure 12. Relationship between runaway current dissipation rate and (a) the runaway current and (b) the injected impurity quantity N_{inj}. Reproduced from [38]. © IOP Publishing Ltd. All rights reserved.

runaway current and quantity of injected impurity, as can be seen in figure 12. However, the dissipation efficiency is saturated with a maximum of 28 MA s^{-1} when the injected impurity quantity exceeds 2×10^{21}. The main reason for this is due to the decrease in the impurity assimilation rate. This result indicates that the assimilation efficiency reaches a stable value even though the injected impurity can be increased continuously. This result is important for the application and design of MGI which is considered in the ITER disruption mitigation system.

4.2. Dissipation of runaway current by ohmic field

The injection of high-Z impurity by the secondary MGI is very efficient in the runaway current decay, but also accelerates the RE beam vertical drift, and the scraping-off of the RE beam by the vertical displacement is found to actively increase the radial electric field that can slow down the runaway current decay [39]. Thus, active and efficient position control of the RE beam is essential for disruption mitigation. Many studies on devices [40–43] have investigated the control of post-disruption runaway current, and similar research is carried out on J-TEXT [44]. The statistical result is illustrated in figure 13. Without optimized horizontal displacement control, the runaway current plateau lasts less than 20 ms; however, it is elongated to more than 80 ms after optimization. Under the control of the RE plateau, dissipation of runaway current by the modulation of $E_{||}$ via an ohmic (OH) field is studied in J-TEXT, as shown in figure 14. Shot #1050017 is reference discharge, and the shots #1050021 and #1050019 are applied by modifying the OH field voltage between about 58 V and –216 V, respectively. A significant decay of runaway current is observed by externally applied negative loop voltages in the experiment. According to simple

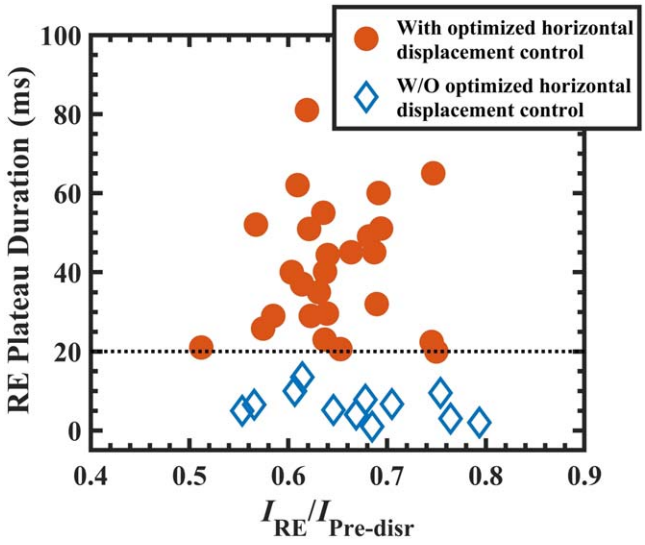

Figure 13. Duration of RE plateau versus ratio of runaway current I_{RE} and pre-disruption plasma current $I_{Pre\text{-}disr}$. Reproduced from [44]. © 2020 Hefei Institutes of Physical Science, Chinese Academy of Sciences and IOP Publishing. All rights reserved.

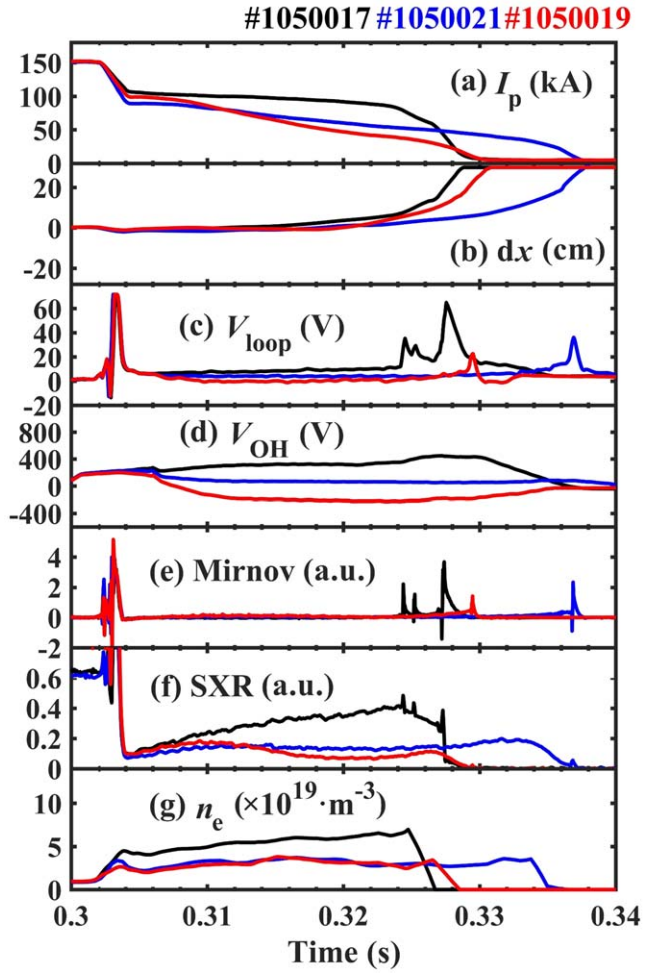

Figure 14. Time of runaway currents with different loop voltage. Reproduced from [44]. © 2020 Hefei Institutes of Physical Science, Chinese Academy of Sciences and IOP Publishing. All rights reserved.

estimation, the decay of runaway current can be achieved when the toroidal electric field is less than 7–12 times the theoretical critical electric field. The dissipation rate of runaway current by the OH field can be up to a maximum value of 3 MA s^{-1}, which is less than the one achieved by MGI. Nevertheless, this way to deplete REs is gentle and maybe a possible auxiliary method for soft landing.

4.3. Dissipation of runaway current by SPI

The study of SPI affecting runaway current dissipation is carried out on J-TEXT. For comparison with the MGI results, the quantity of the SPI injected impurity is similar to that of MGI. The velocity of the pellets can be up to 150–300 m s^{-1} by SPI. In the experiment, the dissipation rate of runaway current reaches 12 MA s^{-1} when the injected Ar quantity is up to 2.12×10^{21}, and this dissipation rate is slower than that of MGI (18 MA s^{-1}) [13], which may be due to the difference in injection speed between SPI and MGI. Comparing the disruption mitigation processes of MGI and SPI, it is found that the cold front of SPI can penetrate the $q = 1$ rational surface and the deposition position is closer to the plasma center [45]. However, the Ar injected by MGI only reaches the $q = 2$ rational surface, as shown in figure 15. Due to the deeper penetration depth of SPI than MGI, a larger quantity of impurities is deposited in the center, leading to the increase in electron density. The time evolution of the electron density for SPI and MGI is shown in figure 16. The core density for the SPI case can reach a higher value than the MGI case, but it has the opposite behavior in the edge density. Moreover, a high impurity assimilation rate can be obtained by changing the pellet velocity in a certain range. The promising features of deep penetration and high assimilation efficiency of impurity are inspiring for applications in the future.

5. Simulation results of RE suppression

Due to the short duration of disruption and the limit of diagnostics, modeling and simulation are developed quickly to explore the physics behind the disruption suppression and mitigation. The NIMROD code [46] has primarily evolved a set of nonlinear single fluid MHD equations, consisting of modified Faraday's law, resistive MHD Ohm's law, and Ampere's law with the low-frequency limit, particle conservation, flow velocity evolution, and temperature evolution, which is applied on the J-TEXT tokamak. In order to be effective for disruption mitigation research, a radiative cooling model KPRAD is added in the extended code in order to simulate more realistic radiation rates during the rapid shutdown phase by MGI. Moreover, the guiding-center drift motion of the test REs and the plasma response of the RMP during the entire disruption process are considered in this module as well. Thus, the RE loss impacted by magnetic perturbations can be sensitively studied by this module. The NIMROD simulations applied in J-TEXT focus on the physics and the mechanism under the disruption mitigation

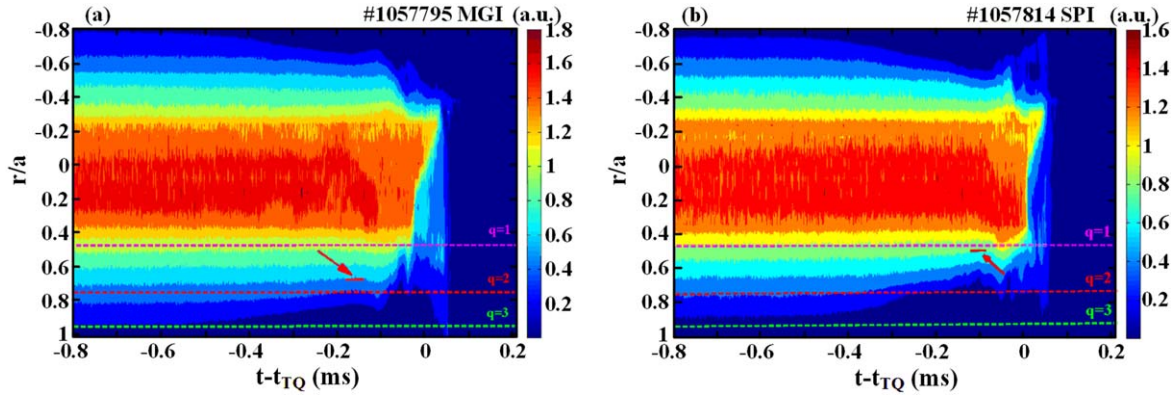

Figure 15. Time evolution of the ECE profile for (a) MGI and (b) SPI. Reproduced courtesy of IAEA. Figure from [45]. Copyright (2021) IAEA.

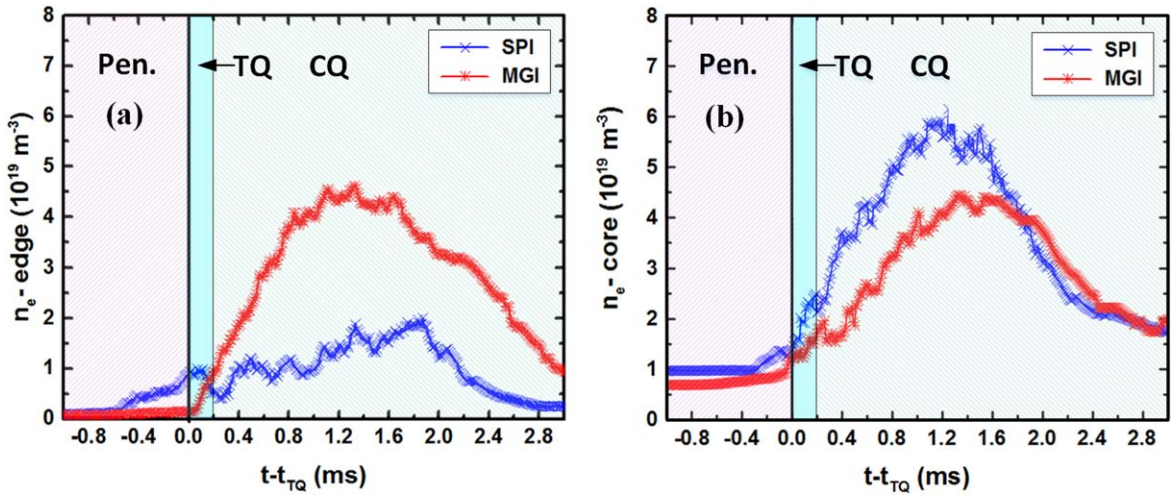

Figure 16. Comparison of the electron density in the plasma (a) edge and (b) center between SPI and MGI. Reproduced courtesy of IAEA. Figure from [45]. Copyright (2021) IAEA.

experiment, consequently helping to optimize the method of disruption mitigation.

In order to verify the experimental results of the locked island phase on the suppression of REs, the realistic magnetic perturbation structure generated by RMP coils is used in the simulation. Figure 17 shows that the confinement of RE seeds can be greatly affected by the $2/1$ mode locked island phases during the TQ phase. The dependence of the ratio of remaining REs on the phase difference between $n = 1$ and locked mode is shown in figure 17(b) [47]. In order to suppress the generation of REs, the optimized relative phase is predicted to be toroidal 90° ($\Delta\varnothing = \varnothing_{\mathrm{MGI}} - \varnothing_{n=1}$). This result can be interpreted by the evolution of magnetic perturbation during disruption, in which the magnetic topology is influenced by the impurity spreading process in different phases. The influence of the width of $2/1$ pre-existing magnetic islands on the RE suppression during disruption is studied in J-TEXT [48]. The magnetic islands are implemented according to the perturbation field presetting in NIMROD. It is observed that there is a non-monotonic tendency between the RE confinement and the width of the $2/1$ pre-existing locked island, which is shown in figure 18. When the width of the $2/1$ pre-existing magnetic islands exceeds $0.3a$ (a is the plasma minor radius), it causes large magnetic perturbation and strong stochasticity of the magnetic surface to expel the REs during disruption. For the small island case, a reduction of about 40% in RE seeds is found in the simulation compared to the case without islands. However, the remaining RE ratio reaches the maximum in the medium island region, which may be due to the smaller duration of magnetic perturbation $\delta B/B$ (exceeding $(4-6)\times 10^{-3}$) and the lower amplitude of high n modes induced during disruption. This evolution of magnetic perturbation is found to be significantly related to the impurity penetration, which shows that the effect of three dimensions between the injected impurities and the $2/1$ locked modes is important for disruption mitigation.

6. Summary and outlook

Effective disruption mitigation is a key issue in the safe and reliable operation of future tokamaks, including ITER. Approaches aimed at suppressing and mitigating runaway current formation by SMBI, RMP, MGI, SPI, MET and OH field have been investigated in J-TEXT. Complete

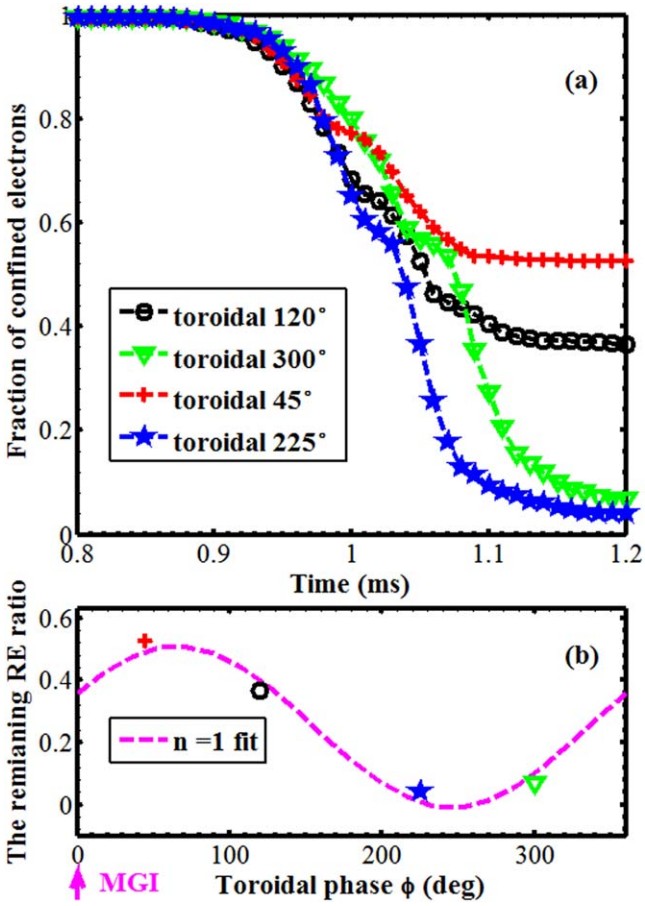

Figure 17. Effect of phases of pre-existing $2/1$ locked islands on RE confinement. (a) Time evolution of fraction of confined REs in four island phases. (b) Dependence of the remaining RE ratio on the toroidal phase of $2/1$ islands. Reprinted from [47], with the permission of AIP Publishing.

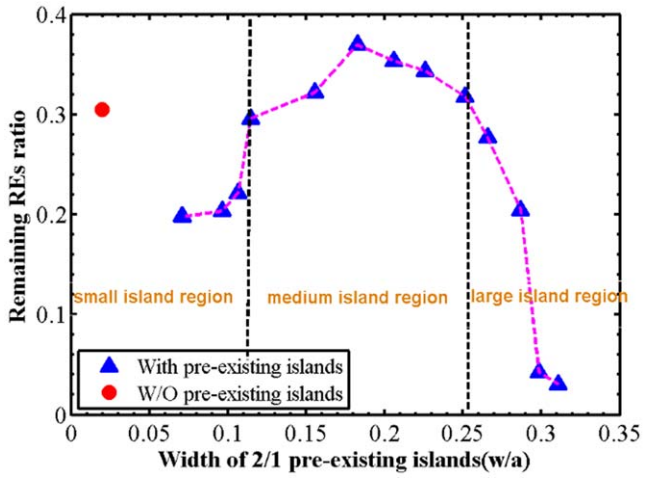

Figure 18. Relationship between the remaining RE ratio and the width of pre-existing $2/1$ locked islands. Reproduced from [48]. © IOP Publishing Ltd. All rights reserved.

suppression of REs is realized by H_2 SMBI with an earlier trigger time or sufficient H_2 quantity, in which SMBI provokes significant magnetic perturbation that destroys the intact magnetic surface in the core and enhances loss of REs during disruption. The large magnetic islands implemented by mode penetration and mode locking can act as explosive bombs during disruptions and lead to stronger stochasticity in the whole plasma cross section, which can completely suppress the REs. The MET system provides another possible auxiliary method to suppress the generation of REs by decreasing the parallel electric field during disruption. When the secondary impurity gas reaches the plasma edge before TQ, the generation of runaway current can be significantly suppressed by the second MGI valve.

For large-scale devices, a cascade strategy for the control of runaway current is essential. Consequently, the runaway current should be robustly dissipated or soft landed to minimize damage to critical components of the device. With the high-Z impurities injected by secondary MGI, runaway current can be significantly dissipated; the dissipation rate increases with the impurity quantity, and reaches a stable value with a maximum of 28 MA s^{-1}. Based on the control of RE beam position, a significant decay of runaway currents is observed in J-TEXT when the toroidal electric field is 7–12 times smaller than the theoretical critical electric field. SPI, as a new disruption mitigating technology, is found to have a deeper penetration and a higher assimilation than MGI, which is inspiring for applications in the future.

In order to understand the underlying disruption mitigation physics, the simulation based on NIMROD is used on J-TEXT. The results show that the RE confinement significantly varies with the phase and size of $2/1$ mode locked islands during the TQ phase. The ratio of remaining REs presents an $n = 1$ dependence on the toroidal phase of the locked islands and shows a non-monotonic tendency on the width of the pre-existing $2/1$ locked islands. The ratio of remaining REs is found to be significantly reduced in the small and large islands; however, it is increased in the medium islands which may be due to the smaller duration of magnetic perturbation $\delta B/B$ (exceeding $(4-6)\times 10^{-3}$) and the low amplitude of high n modes induced during disruption.

Due to the uncertainty in the disruption mitigating system applied in ITER, future work on J-TEXT will continually focus on exploring the technology availability and the physics behind disruption, such as the SPI disruption mitigation and alternative means of RE mitigation.

Acknowledgments

This work is supported by the National MCF Energy R & D Program of China (Nos. 2019YFE03010004, 2018YFE0309103, 2018YFE0310300, 2018YFE0309100, 2017YFE0302000, 2017YFE0300501), National Natural Science Foundation of China (Nos. 11775089, 51821005, 12205122, 11905077 and 11575068), and the Natural Science Foundation of the Jiangsu Higher Education Institutions of China (No. 21KJB140025).

References

[1] Lehnen M *et al* 2015 *J. Nucl. Mater.* **463** 39
[2] ITER Physics Expert Group on Disruptions *et al* 1999 *Nucl. Fusion* **39** 2251
[3] Riccardo V *et al* 2010 *Plasma Phys. Control. Fusion* **52** 124018
[4] Reux C *et al* 2010 *Nucl. Fusion* **50** 095006
[5] Lehnen M *et al* 2011 *Nucl. Fusion* **51** 123010
[6] Commaux N *et al* 2016 *Nucl. Fusion* **56** 046007
[7] Martín-Solís J R, Loarte A and Lehnen M 2017 *Nucl. Fusion* **57** 066025
[8] Granetz R S *et al* 2014 *Phys. Plasmas* **21** 072506
[9] Zhuang G *et al* 2013 *Nucl. Fusion* **53** 104014
[10] Luo Y H *et al* 2014 *Rev. Sci. Instrum.* **85** 083504
[11] Rao B *et al* 2014 *Fusion Eng. Des.* **89** 378
[12] Liang Y *et al* 2019 *Nucl. Fusion* **59** 112016
[13] Li Y *et al* 2018 *Rev. Sci. Instrum.* **89** 10K116
[14] Xiao J S *et al* 2015 *J. Fusion Energy* **34** 1020
[15] Zhang M *et al* 2016 *Fusion Eng. Des.* **109–11** 975
[16] Cai N H *et al* 2021 *Fusion Eng. Des.* **169** 112488
[17] Chen J *et al* 2014 *Rev. Sci. Instrum.* **85** 11D303
[18] Guo D J *et al* 2017 *Rev. Sci. Instrum.* **88** 123502
[19] Yang Z J *et al* 2012 *Rev. Sci. Instrum.* **83** 10E313
[20] Yang Z J *et al* 2016 *Rev. Sci. Instrum.* **87** 11E112
[21] Chen Z Y *et al* 2012 *Rev. Sci. Instrum.* **83** 056108
[22] Tong R H *et al* 2018 *Rev. Sci. Instrum.* **89** 10E113
[23] Breizman B N *et al* 2019 *Nucl. Fusion* **59** 083001
[24] Connor J W and Hastie R J 1975 *Nucl. Fusion* **15** 415
[25] Dreicer H 1960 *Phys. Rev.* **117** 329
[26] Smith H M and Verwichte E 2008 *Phys. Plasmas* **15** 072502
[27] Rosenbluth M N and Putvinski S V 1997 *Nucl. Fusion* **37** 1355
[28] Hollmann E M *et al* 2010 *Phys. Plasmas* **17** 056117
[29] Liu C *et al* 2018 *Nucl. Fusion* **58** 096030
[30] Spong D A *et al* 2018 *Phys. Rev. Lett.* **120** 155002
[31] Paz-Soldan C *et al* 2019 *Nucl. Fusion* **59** 066025
[32] Zeng L *et al* 2013 *Phys. Rev. Lett.* **110** 235003
[33] Commaux N *et al* 2011 *Nucl. Fusion* **51** 103001
[34] Huang D W *et al* 2017 *Plasma Phys. Control. Fusion* **59** 085002
[35] Chen Z Y *et al* 2018 *Nucl. Fusion* **58** 082002
[36] Lin Z F *et al* 2019 *Plasma Phys. Control. Fusion* **61** 024005
[37] Wei Y N *et al* 2019 *Plasma Phys. Control. Fusion* **61** 084003
[38] Wei Y N *et al* 2020 *Plasma Phys. Control. Fusion* **62** 025002
[39] Konovalov S *et al* 2016 *Proc. of 2016 IAEA Fusion Energy Conf. (Kyoto)* (Vienna: IAEA)
[40] Fredrickson E D *et al* 2015 *Nucl. Fusion* **55** 013006
[41] Eidietis N W *et al* 2012 *Phys. Plasmas* **19** 056109
[42] Carnevale D *et al* 2019 *Plasma Phys. Control. Fusion* **61** 014036
[43] Ficker O *et al* 2019 *Nucl. Fusion* **59** 096036
[44] Hu J *et al* 2020 *Plasma Sci. Technol.* **22** 115102
[45] Li Y *et al* 2021 *Nucl. Fusion* **61** 126025
[46] Sovinec C R *et al* 2004 *J. Comput. Phys.* **195** 355
[47] Jiang Z H *et al* 2019 *Phys. Plasmas* **26** 062508
[48] Li C H *et al* 2020 *Plasma Phys. Control. Fusion* **62** 095010